Journal of Medicinal Chemistry

Article

pubs.acs.org/jmc

# Studies on an (*S*)-2-Amino-3-(3-hydroxy-5-methyl-4-isoxazolyl)propionic Acid (AMPA) Receptor Antagonist IKM-159: Asymmetric Synthesis, Neuroactivity, and Structural Characterization

Lina Juknaitė,[‖] Yutaro Sugamata,[†] Kazuya Tokiwa,[†] Yuichi Ishikawa,[†] Satoshi Takamizawa,[†] Andrew Eng,[‡] Ryuichi Sakai,[§] Darryl S. Pickering,[‖] Karla Frydenvang,[‖] Geoffrey T. Swanson,[‡] Jette S. Kastrup,[‖] and Masato Oikawa*[,†]

[†]Graduate School of Nanobioscience, Yokohama City University, Seto 22-2, Kanazawa-ku, Yokohama 236-0027, Japan

[‡]Department of Molecular Pharmacology and Biological Chemistry, Northwestern University Feinberg School of Medicine, 303 East Chicago Avenue, Chicago, Illinois 60611, United States

[§]Faculty of Fisheries Sciences, Hokkaido University, Hakodate 041-8611, Japan

[‖]Department of Drug Design and Pharmacology, Faculty of Health and Medical Sciences, University of Copenhagen, DK-2100 Copenhagen Ø, Denmark

Supporting Information

**ABSTRACT:** IKM-159 was developed and identified as a member of a new class of heterotricyclic glutamate analogues that act as AMPA receptor-selective antagonists. However, it was not known which enantiomer of IKM-159 was responsible for its pharmacological activities. Here, we report in vivo and in vitro neuronal activities of both enantiomers of IKM-159 prepared by enantioselective asymmetric synthesis. By employment of (*R*)-2-amino-2-(4-methoxyphenyl)ethanol as a chiral auxiliary, (2*R*)-IKM-159 and the (2*S*)-counterpart were successfully synthesized in 0.70% and 1.5% yields, respectively, over a total of 18 steps. Both behavioral and electrophysiological assays showed that the biological activity observed for the racemic mixture was reproduced only with (2*R*)-IKM-159, whereas the (2*S*)-counterpart was inactive in both assays. Racemic IKM-159 was crystallized with the ligand-binding domain of GluA2, and the structure revealed a complex containing (2*R*)-IKM-159 at the glutamate binding site. (2*R*)-IKM-159 locks the GluA2 in an open form, consistent with a pharmacological action as competitive antagonist of AMPA receptors.

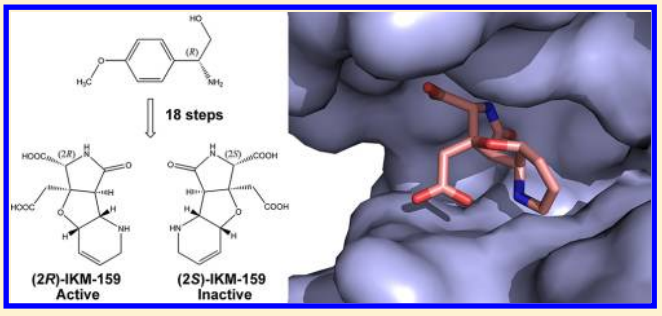


## INTRODUCTION

Ionotropic glutamate receptors (iGluRs) mediate the majority of fast excitatory neurotransmission in the mammalian central nervous system (CNS) and play an important role in higher brain functions such as learning and memory.[1] iGluRs are also thought to be involved, fully or partly, in nociception and closely related to several brain disorders such as epilepsy, ischemia-induced excitotoxicity, and Alzheimer, Huntington, and Parkinson diseases.[2−5] Structurally, iGluRs are assembled as homomers or heteromers composed of four subunits that belong to same subunit classes. A total of 18 structurally diverse iGluR subunit superfamily proteins have been identified in the mammalian CNS.[6] One of the major interests in neurochemistry is, therefore, to discover specific ligands to control biological functions of iGluRs selectively, thereby establishing the molecular basis of structurally diverse iGluRs.

Recently, we developed a series of synthetic heterotricyclic glutamate analogues as subtype-selective antagonists for the (*S*)-2-amino-3-(3-hydroxy-5-methyl-4-isoxazolyl)propionic acid (AMPA) type iGluR.[7−10] The structures were originally inspired by the marine natural products kainic acid (KA, **1**, Figure 1)[11] and neodysiherbaine,[2] and we further characterized the pharmacological profile of the most potent molecule, IKM-159.[9] The activities of natural templates and the synthetic

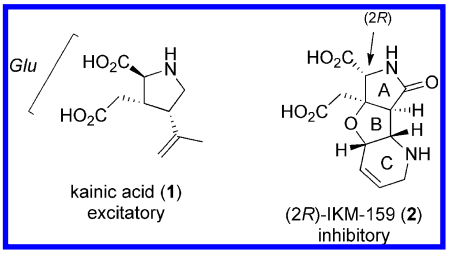


**Figure 1.** Excitatory glutamate analogue kainic acid (**1**)[11] and (2*R*)-IKM-159 (**2**). The (2*R*)-enantiomer was found to be responsible for the antagonist activity of IKM-159 in the present study.

**Received:** October 28, 2012
**Published:** February 23, 2013

**Scheme 1. Construction of Optically Active Oxanorbornenes by Tandem Ugi/Diels–Alder Reaction Using Chiral Amine 3**

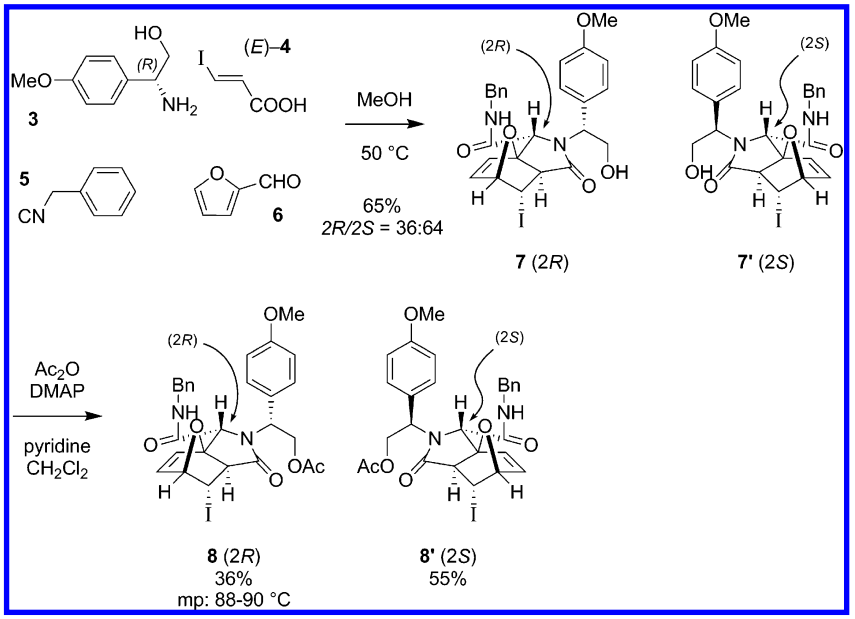


compounds toward iGluRs were found to be significantly different; for example, IKM-159 selectively antagonized AMPA receptors[9] whereas kainic acid is an agonist for both AMPA and KA-type iGluRs.[12]

To acquire additional insight into the mode of interaction between IKM-159 and AMPA receptors, we studied the structure–activity relationships of several synthetic analogues of IKM-159.[9,13] However, previous biological studies were performed only on the racemates because no pathway was available for asymmetric synthesis. Here we report the first asymmetric synthesis and biological evaluation of both enantiomers of IKM-159. We show that (2*R*)-IKM-159 (**2**) is neuronally active, whereas the (2*S*)-counterpart (**20**) is inactive, and further provide structural insight into the binding mode of (2*R*)-IKM-159 with the GluA2 AMPA receptor ligand-binding domain (LBD). The observation in the present structure–activity relationship study of optical isomers of IKM-159 affords new insight into an unconventional mode of interaction between antagonists with this novel chemical template and AMPA receptors.

## RESULTS AND DISCUSSION

**Chemical Synthesis.** The asymmetric synthesis was carried out on the basis of our route for 12 glutamate analogues,[7−10] which was thereafter extended to the racemic IKM-159.[9,13]

To synthesize both enantiomers, we screened chiral amines used for tandem Ugi/Diels–Alder reaction. Among the benzylic amines tested, 2-amino-2-(4-methoxyphenyl)ethanol (**3**)[14] was found to be the most efficient in terms of (1) the stability throughout the synthesis, (2) the formation of crystalline derivative used for structural analysis, and (3) high reactivity toward oxidation for the removal at the final stage. The commercially available desmethoxy analogue, 2-amino-2-phenylethanol, was less practical because of its resistance to the removal under a variety of conditions (see below).

By use of (*R*)-amine **3** prepared in 48% yield over five steps from (*R*)-(4-hydroxyphenyl)glycine,[14] an oxanorbornene framework was readily constructed by a tandem reaction with benzyl isocyanide (**5**),[15,16] 2-furfural (**6**), and (*E*)-iodoacrylic acid (**4**)[17] (Scheme 1). For the carboxylic acid component, the (*E*)-isomer **4** was chosen because the product was expected to be obtained as crystals from our previous study.[13] In this domino reaction, an inseparable mixture of diastereomers **7** (2*R*) and **7′** (2*S*) was obtained in 65% yield (IKM-159 numbering; see Figure 1). The ratio of **7** (2*R*) and **7′** (2*S*) was 36:64. The structures were determined as follows. Acetylation (acetic anhydride ($Ac_2O$), 4-dimethylaminopyridine (DMAP), pyridine) of a mixture of **7** (2*R*) and **7′** (2*S*) furnished two acetates **8** (2*R*) and **8′** (2*S*), which were fortunately separated by carefully performing silica gel column chromatography, in 36% and 55% yields, respectively. The diastereomer that was less polar on thin-layer chromatography was the minor product and was further purified by recrystallization ($Et_2O$, mp 88–90 °C). We successfully determined the crystal structure of the minor product as **8** (2*R*) by single-crystal X-ray analysis at 183 K. The ORTEP drawing [Burnett, M. N.; Johnson, C. K. *ORTEP-III: Oak Ridge Thermal Ellipsoid Plot Program for Crystal Structure Illustrations*; Report ORNL-6895; Oak Ridge National Laboratory: Oak Ridge, TN, 1996] is shown in Figure 2. Both isomers **8** (2*R*) and **8′** (2*S*) independently led to optically active IKM-159 as follows.

Scheme 2 shows a so-called ring-rearrangement metathesis[18] of the oxanorbornene framework leading to optically active heterotricycle **13**. *N*-Ns amine (Ns = 2-nitrobenzenesulfonyl)[19,20] **10** was synthesized in 70% yield by reaction of iodide **8** (2*R*) with *N*-Ns-allylamine (**9**)[21] and $Cs_2CO_3$ at 50 °C. The stereochemistry was determined on the basis of $^3J_{H4,H5}$ (3.6 Hz), which was consistent with that of the corresponding intermediate for the synthesis of racemic IKM-159.[13] Although the reaction took place with a retention of configuration at C5, the mechanism can be reasonably understood as a sequence of elimination of hydrogen iodide followed by 1,4-conjugate addition of **9**, from a less-hindered *endo* face.[22] The reaction also produced a trace amount of aromatized product (structure not shown). Oxanorbornene **10** was then converted efficiently into heterotricycle **12** by domino metathesis reaction in one step, using Hoveyda–Grubbs second-generation catalyst **11**.[23] Thus, the reaction was conducted with vinyl acetate in benzene at 60 °C to provide heterotricycle **12** (*E*/*Z* = 6:4) in 71% yield


dx.doi.org/10.1021/jm301590z | J. Med. Chem. 2013, 56, 2283–2293

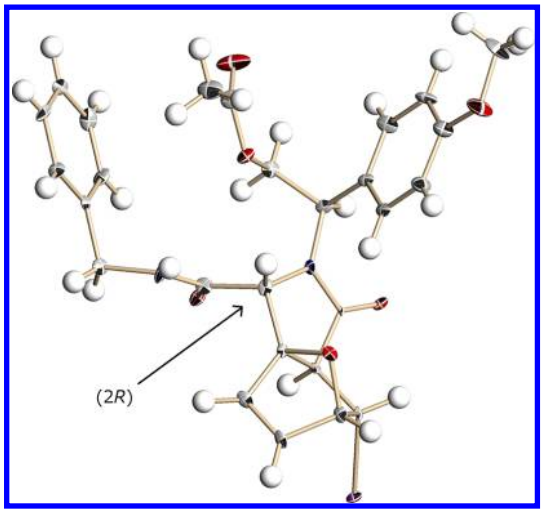


**Figure 2.** Thermal ellipsoid drawing of the asymmetric molecular unit at the 50% probability level of **8** (2*R*) at 183 K. Elements are color-coded: C (gray), H (white), I (purple), N (blue), and O (red).

**Scheme 2. Ring-Rearrangement Metathesis of Oxanorbornene Framework Leading to Optically Active Heterotricycle 13**

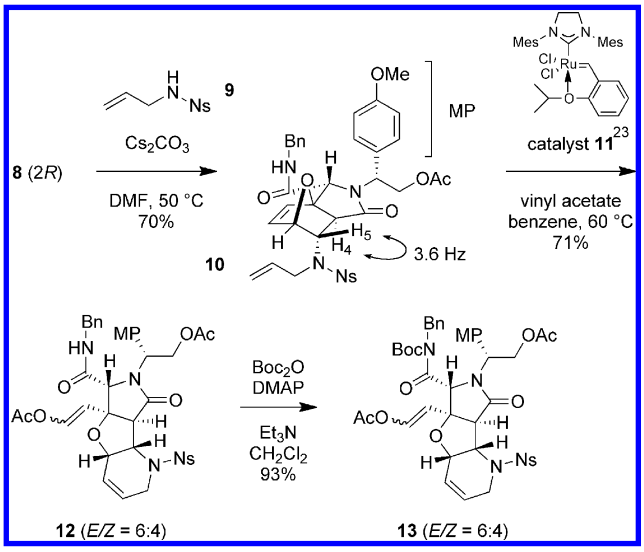


with quantitative recovery of unreacted oxanorbornene **10**, which was again used for the metathesis. Next, heterotricycle **12** was treated with $Boc_2O$ (Boc = *tert*-butoxycarbonyl), DMAP, and triethylamine to afford *N*-Boc-imide **13** (*E*/*Z* = 6:4) in 93% yield so that transformation to the methyl ester in the next step could be performed under mild conditions.

Methanolysis of **13** was performed by $K_2CO_3$ in methanol at −10 °C to generate aldehydes (**14A**, **14B**) and (*Z*)-vinyl carbonates (**15A**, **15B**) as an inseparable mixture in the ratio of 26:11:31:32, as estimated from $^1H$ NMR (Scheme 3). Alcohols **14B** and **15B** were produced by decomposition of the Ac group under the alkaline conditions. Many attempts to suppress the undesired byproducts (**14B**, **15A**, **15B**) were unsuccessful. For example, the use of $Li_2CO_3$ for the base resulted in no reaction even at elevated temperature. It is notable that methanolysis also produced unexpected vinyl carbonates (**15A**, **15B**), which were generated solely as the thermodynamically unfavorable (*Z*)-isomer, as judged from the $^3J_{H,H}$ (7.2 Hz). The product ratio between desired aldehyde (**14A**, **14B**) and undesired (*Z*)-

**Scheme 3. Alkaline Methanolysis Unexpectedly Provides a Complex Mixture**

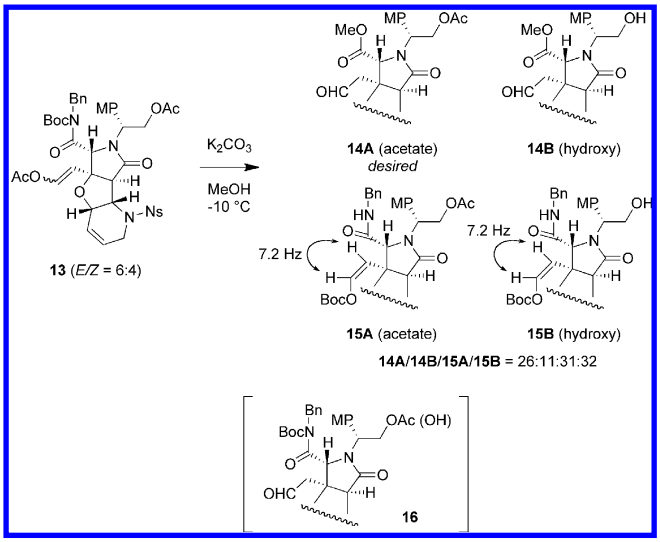


vinyl carbonates (**15A**, **15B**) could not be controlled, and only a poor reproducibility was observed, while the substrate **13** was rapidly consumed after 1.5 h.

The geometry of the vinyl group apparently indicated that the (*Z*)-vinyl carbonate was produced by intramolecular migration of the Boc group from the amide group to the intimate enol group. The independence of the product distribution on the *E*/*Z* ratio (6:4) of the reaction substrate **13** may indicate that the reaction proceeds via the intermediary aldehyde **16**, which is not detected yet. However, the mechanism is likely complicated judging from the poor reproducibility observed (see above). Although the methanolysis provided a complex mixture of products, the synthetic study was continued using the mixture without purification or separation, as follows.

After Pinnick oxidation ($NaClO_2$, 2-methyl-2-butene, $NaH_2PO_4$)[24] of the methanolysis mixture (**14A**, **14B**, **15A**, **15B**), the resulting carboxylic acid was esterified with trimethylsilyldiazomethane (TMS-$CHN_2$) to give dimethyl ester (Scheme 4). Without purification, acetylation of the

**Scheme 4. A Series of Functional Group Transformations, Successfully Performed on the Methanolysis Mixture (14A, 14B, 15A, 15B), Provided Two Products 15A and 17**

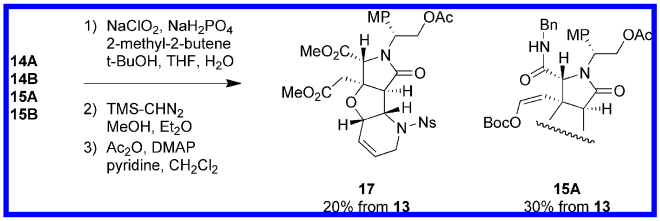


hydroxy group on the chiral auxiliary, which had been partially generated by methanolysis, was performed. These transformations successfully culminated to give rise to two products, the desired diester **17** and (*Z*)-vinyl carbonate (**15A**) in 20% and 30% yields (from **13**), respectively, after chromatographic purification. No other notable product was observed. The results indicate that Pinnick oxidation, TMS-$CHN_2$ treatment, and acetylation have proceeded with high chemoselectivity.


dx.doi.org/10.1021/jm301590z | J. Med. Chem. 2013, 56, 2283−2293

Transformation of **15A** into the reusable aldehyde such as **16** is under investigation.

Chiral auxiliary was then oxidatively removed by ceric ammonium nitrate (CAN) at 0 °C to afford *N*-monoalkylamide **18** in 90% yield (Scheme 5). The reaction proceeded as

**Scheme 5. Final Elaboration toward (2*R*)-IKM-159 (2)**

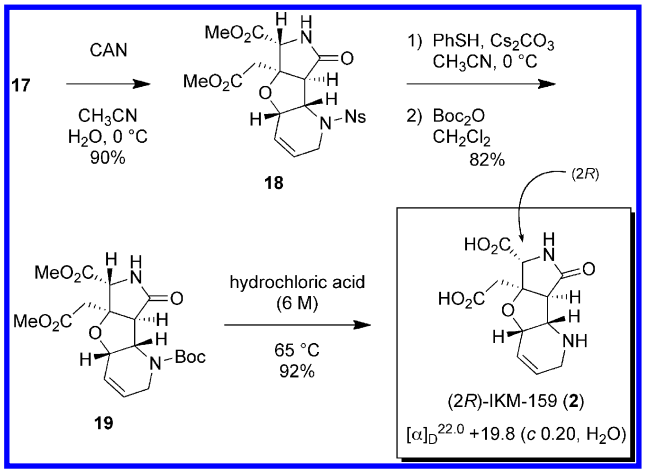


expected from our previous synthetic study of artificial glutamates,[10] wherein the 4-methoxybenzyl group had been removed at −10 °C in 71−80% yield. Of interesting note, we found that the acetyl and methoxy groups in **17** were indispensable for the reaction because the desmethoxy counterpart of **17**, derived from commercially available 2-amino-2-phenylethanol, could not be deprotected under a variety of conditions using reagents such as CAN, 2,3-dichloro-5,6-dicyano-*p*-benzoquinone (DDQ), $H_2$/Pd,[25] $O_2$/NaOH,[26] and free radical. Similarly, the auxiliary could not be removed with CAN before acetylation. Chromatographic and spectroscopic data of **18** were identical to those for the racemate.[10,13] To purify thoroughly by chromatography, the Ns group in **18** was then replaced with a Boc group by two-step transformation (PhSH, $Cs_2CO_3$, then $Boc_2O$) to give *N*-Boc-amine **19** in 82% yield.[7,10] Finally, all protecting groups were simultaneously removed by hydrolysis with 6 M hydrochloric acid at 65 °C to give rise to (2*R*)-IKM-159 (**2**) in 92% yield. Chromatographic and spectroscopic data of **2** were completely identical to those of racemic IKM-159.[13] The yield from **8** (2*R*) was 6.3% over 11 steps, and the total yield was 0.70% over 18 steps from (*R*)-(4-hydroxyphenyl)glycine by way of **8** (2*R*). The enantiomeric (2*S*)-IKM-159 (**20**) was also synthesized using the same reaction sequence starting from (*R*)-(4-hydroxyphenyl)glycine by way of **8′** (2*S*), in 1.5% yield over 18 steps (Figure 3). The values of optical rotation for both enantiomers were found to be consistent: $[\alpha]_D^{22.0}$ +19.8 (*c* 0.20, $H_2O$) for (2*R*)-IKM-159 (**2**) and $[\alpha]_D^{20.9}$ −19.8 (*c* 0.16, $H_2O$) for (2*S*)-IKM-159 (**20**).

**Biological Evaluation.** Biological activity of both (2*R*)- and (2*S*)-IKM-159 was next tested in mice. The drug was injected intracerebroventricularly at five doses ranging from 0.7 to 355 nmol/mouse. Injection of (2*R*)-IKM-159 (KT1-121-2, 355 nmol/mouse) caused flaccidness in mice, while the antipode (2*S*)-IKM-159 (SG1-146-2, 355 nmol/mouse) did not show significant activity. Though the behavioral phenotype observed here was similar to that reported for the racemic mixture, a dose-dependent profile of the compound was not previously determined. The highest dose (355 nmol/mouse) caused mice to become totally flaccid, and their righting reflex was lost for

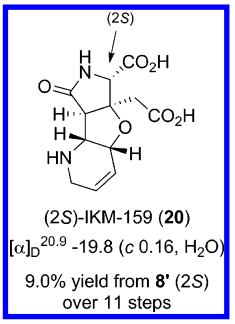


**Figure 3.** (2*S*)-IKM-159 (**20**), synthesized from diastereomeric oxanorbornene **8′** (2*S*).

up to 4 h. Occasional and transient stereotyped behaviors such as scratching were observed. Flaccidity was produced in all mice tested at higher doses (>35 nmol/mouse), and the latency was proportional to the dose injected. A lower dose of (2*R*)-IKM-159 (7 nmol/mouse) produced variable responses, with one animal losing the righting reflex and two others exhibiting catalepsy and ataxia during recovery from drug effects. These characteristic behavioral phenotypes were scored as follows: flaccidness lasting for >4 h (score 7), 2−4 h (score 6), 1−2 h (score 5), <1 h (score 4); catalepsy (score 3); loss of voluntary movement (200% of control, score 2; 150−200% of control, score 1; same as control, score 0). A dose−response curve generated from the fitted curve from five data points using three mice at each data point yielded an $ED_{50}$ for (2*R*)-IKM-159 of 6.3 (3.5−11.4) nmol/mouse.

Racemic IKM-159 was characterized as an AMPA receptor antagonist.[9] This observation was consistent with its behavioral activity because other AMPA receptor antagonists, including the noncompetitive benzodiazepine GYKI52466 and its analogues[27] as well as the competitive quinoxaline ZK200775,[28] induce muscle relaxation and ataxia similar to IKM-159. To confirm that (2*R*)-IKM-159 was the enantiomer responsible for AMPA receptor antagonism, we tested both (2*R*) and (2*S*) compounds in whole-cell patch clamp recordings of AMPA receptor excitatory postsynaptic currents (EPSCs) from cultured rat hippocampal neurons (Figure 4). *N*-Methyl-D-aspartic acid (NMDA) and γ-aminobutyric acid type A ($GABA_A$) receptor currents were inhibited using respective antagonists (see the Supporting Information). Under these conditions, AMPA receptors mediated very-large-amplitude bursts of synaptic currents. Representative traces in the figure show that AMPA receptor-mediated EPSCs were profoundly reduced by (2*R*)-IKM-159 but were unaffected by the (2*S*)-enantiomer (both tested at 20 μM), which was confirmed by quantitation of the mean charge transfer during spontaneous EPSCs ((2*R*), 16 ± 7% of control charge transfer; (2*S*), 96 ± 13%; $n$ = 4 recordings for each compound; ∗, $p < 0.05$ in a paired $t$ test). Thus, (2*R*)-IKM-159 is responsible for both the behavioral and pharmacological activity of the racemate.

**Structure Determination.** Racemic IKM-159 was postulated to be a competitive AMPA receptor antagonist based on a preliminary pharmacological analysis, although some uncertainty in this conclusion existed because relatively high concentrations (100 μM) of the racemate did not displace radioligand from the orthosteric binding site on recombinant AMPA receptors.[9] In order to clarify the mechanism of action and to gain insight into the molecular basis for the action of this chemically novel antagonist, we used X-ray crystallography to solve the structure of IKM-159 (from the racemic mixture)


dx.doi.org/10.1021/jm301590z | J. Med. Chem. 2013, 56, 2283−2293

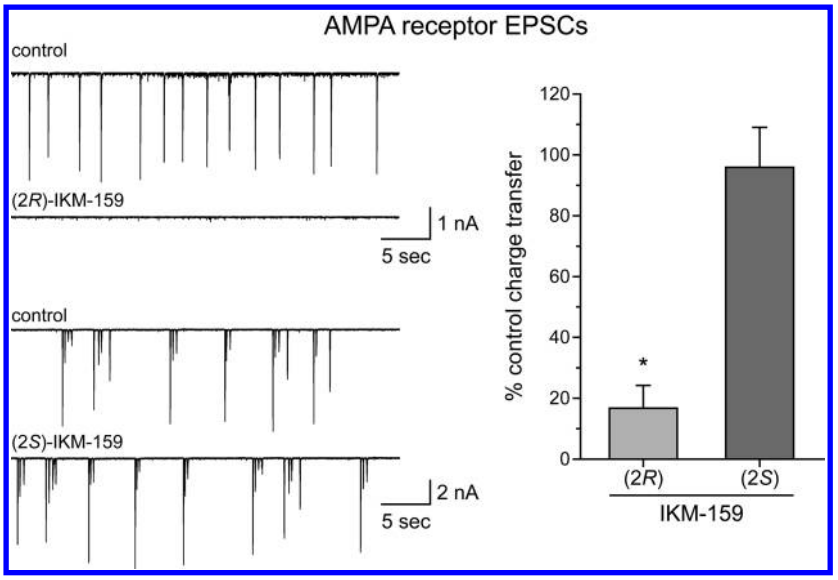


**Figure 4.** AMPA receptor excitatory synaptic currents (EPSCs) recorded from rat hippocampal neurons are inhibited by (2*R*)- but not (2*S*)-IKM-159 (20 $\mu$M). Representative traces are shown on the left. Quantitation of the charge transfer in the presence of the IKM-159 compounds as a percentage of their respective predrug activities is shown on the right. (2*R*)-IKM-159 reduced charge transfer significantly, whereas (2*S*) was inactive ($n$ = 4 for each condition; *, $p < 0.05$).

with the GluA2 LBD to 2.3 Å resolution (Table 1). Two dimers (A/C and B/D) were found in the asymmetric unit of the crystal, each dimer existing as a mixed dimer of one molecule containing (2*R*)-IKM-159 in the binding site (molecules A and B) and the other molecule a sulfate or phosphate ion (modeled as sulfate; molecules C and D) (see Figure 5A). The D1–D2 domain opening in GluA2 with (2*R*)-IKM-159 relative to the glutamate bound structure (PDB code 1FTJ,[29] molB) is 20.1° in molecule A and 20.0° in molecule B, similar to that seen in the apo structure of GluA2 LBD (PDB code 1FTO).[29] Partial domain opening is seen in the two GluA2 molecules containing a sulfate ion, i.e., 13.1° in molecule C and 11.9° in molecule D. The distance between the two artificial Gly-Thr linker regions connecting segments S1 and S2, as measured between Ile654 of each molecule of the dimer, is 27.6 Å in the A/C dimer and 27.5 Å in the B/D dimer, which is comparable to the GluA2 LBD apo structure and other antagonist bound structures.[30]

The binding affinity ($K_i$) of racemic IKM-159 at GluA2 LBD, which is predominantly a monomer in solution, was found to be 0.21 ± 0.02 mM ($n$ = 3) with Hill coefficient $n_H$ = 1.03 ± 0.09. Thus, the binding affinity of racemic IKM-159 at the GluA2 glutamate binding site is low and comparable to that at the GluA2$(R)_o$ full-length receptor ($K_i$ = 0.56 ± 0.07 mM, $n_H$ = 1.01 ± 0.07 ($n$ = 3)). (2*R*)-IKM-159 makes several polar contacts to GluA2 binding site residues (Figure 5B–D). These contacts are the same in molecules A and B. The $\alpha$-carboxylate group of (2*R*)-IKM-159 forms contacts with the side chain guanidinium group of Arg506 and the backbone nitrogen of Thr501, similar to what has previously been seen for other amino acid containing antagonists.[30] The $\alpha$-nitrogen atom in (2*R*)-IKM-159 donates one hydrogen bond to the backbone carbonyl oxygen of Pro499. The positively charged secondary amine in the six-membered ring of (2*R*)-IKM-159 attracts the $\gamma$-carboxylate group of Glu726 to form a salt bridge and also forms an intramolecular salt bridge to the distal carboxylate of (2*R*)-IKM-159. The distal carboxylate of (2*R*)-IKM-159 in addition makes a hydrogen bond with the backbone nitrogen of Ser675. Finally, the amide carbonyl oxygen forms a hydrogen bond to the side chain hydroxyl group of Tyr753.

In the binding cavity of molecule A with (2*R*)-IKM-159 bound, three water molecules within 3.5 Å of (2*R*)-IKM-159 could be unambiguously modeled, one of which forms a direct hydrogen bond to (2*R*)-IKM-159 (W1, Figure 5B). This water molecule interacts with the distal carboxylate of (2*R*)-IKM-159 and is also seen in molecule B. The second water molecule (W2) forms a close contact to the secondary amine of (2*R*)-IKM-159. As only very weak density for this water molecule was observed in molecule B, it was not modeled into the binding site of molecule B. The third water molecule (W3) is located in the vicinity of Glu423 and Thr707, which in agonist bound structures form an important interdomain hydrogen bond.[30] In molecule B, this water molecule is not seen because of a different conformation of Glu423 (Figure 6B). Five additional water molecules were located within 3.5 Å of (2*R*)-IKM-159 in molecule B, denoted W4–W8 (Figure 5C). As only very weak density for these water molecules was observed in molecule A, they were not modeled into the binding site of molecule A. Water molecules W4–W6 form polar contacts to (2*R*)-IKM-159: W4 to the distal carboxylate, W5 to the carbonyl oxygen and the $\alpha$-nitrogen, and W6 to the $\alpha$-carboxylate (last contact not shown in Figure 5C). Finally, W7 forms hydrogen bonds to Thr707 and Tyr723, and W8 forms hydrogen bonds to Thr501 and Ser675 (contacts not shown). A putative chloride ion is located in the binding site of molecules A and B, ~4 Å from (2*R*)-IKM-159 (not shown). Finally, in the partially closed molecules C and D, the sulfate ion forms a salt bridge to the side chain guanidinium group of Arg506 in D1 and hydrogen-bonds to the backbone nitrogen and side chain hydroxyl group of Ser675 in D2 (Figure 5E).

The structure of GluA2 LBD with (2*R*)-IKM-159 was compared to other GluA2 LBD structures with antagonists and was found to mostly resemble the GluA2 LBD structures with (*S*)-2-amino-3-[5-*tert*-butyl-3-(phosphonomethoxy)-4-isoxazolyl]propionic acid ((*S*)-ATPO)[32] (PDB code 1N0T) and ZK200775[33] (PDB code 3KGC). Whereas the ring systems


dx.doi.org/10.1021/jm301590z | J. Med. Chem. 2013, 56, 2283–2293

**Table 1. Data Collection and Refinement Statistics of GluA2 LBD in Complex with (2*R*)-IKM-159**

| parameter | GluA2 LBD with (2*R*)-IKM-159 |
|---|---|
| Data | |
| space group | $P2_12_12_1$ |
| unit cell dimensions | |
| *a* (Å) | 62.5 |
| *b* (Å) | 88.8 |
| *c* (Å) | 194.5 |
| molecules (au)[a] | 4 |
| resolution (Å) | 29.2−2.3 (2.42−2.30)[b] |
| no. of unique reflections | 48090 (6547) |
| average redundancy | 3.9 (2.9) |
| completeness (%) | 98.3 (93.2) |
| $R_{merge}$ [c] (%) | 5.6 (12.8) |
| $I/\sigma(I)$ | 9.5 (5.2) |
| Refinement | |
| amino acid residues | 1036 |
| (2*R*)-IKM-159 | 2 |
| water/sulfate ions/chloride ions | 446/6/8 |
| $R_{work}$ (%)[d] | 18.5 |
| $R_{free}$ (%)[e] | 25.8 |
| rmsd on bond lengths (Å)/angles (deg) | 0.007/1.0 |
| residues in allowed regions of Ramachandran plot (%)[f] | 100 |
| *B* (Å$^2$) | |
| Wilson | 21 |
| protein (MolA/MolB/MolC/MolD) | 23/23/24/22 |
| (2*R*)-IKM-159 | 22/21 |
| water/sulfate ions/chloride ions | 23/46/49 |

[a]au: asymmetric unit of the crystal. [b]Values in parentheses correspond to the outermost resolution shell. [c]$R_{merge} = \sum_h\sum_i|I_i(h) - \langle I(h)\rangle|/\sum_h\sum_i(h)$, where $I_i(h)$ is the *i*th measurement. [d]$R_{work} = \sum_{hkl}(||F_{o,hkl}| - |F_{c,hkl}||)/|F_{o,hkl}|$, where $|F_{o,hkl}|$ and $|F_{c,hkl}|$ are the observed and calculated structure factor amplitudes. [e]$R_{free}$ is equivalent to $R_{work}$ but calculated with reflections omitted from the refinement process (5% of reflections omitted). [f]The Ramachandran plot was calculated according to PROCHECK.[31]

in the three antagonists are located differently, the distal carboxylate of (2*R*)-IKM-159 is located in the same region of lobe D2 (Ser675 and Thr676) as the phosphonate groups of (*S*)-ATPO and ZK200775 (Figure 6). However, the phosphonate groups of (*S*)-ATPO and ZK200775 form a more extensive network of interactions than the distal carboxylate of (2*R*)-IKM-159. In (*S*)-ATPO (Figure 6C) and ZK200775 (Figure 6D) the phosphonate group forms a close contact to the γ-carboxylate of Glu726, whereas in the structure with (2*R*)-IKM-159 (Figure 6B) Glu726 interacts with the secondary amine of (2*R*)-IKM-159. The side chain of Glu726 in the structure with (*S*)-ATPO adopts a conformation resembling the conformation in structures with agonists[30] and thereby forms polar contacts to the ammonium group of (*S*)-ATPO and to Tyr753. As Glu726 points away from Tyr753 in the structures with (2*R*)-IKM-159 and ZK200775, these hydrogen bonds are not present in these structures. Instead, the carbonyl oxygen of (2*R*)-IKM-159 makes a hydrogen bond to Tyr753, and in the structure with ZK200775 a contact is formed between Tyr753 and a water molecule. In addition, the binding of (2*R*)-IKM-159 sequesters the water molecule (W3) bridging Glu423 and Thr707, which is not present in the structures with (*S*)-ATPO and ZK200775. This leads to a different conformation of Glu423 in the structure with (2*R*)-IKM-159 compared to the two other structures.

The observation that (2*R*)-IKM-159 binds to the GluA2 LBD structure supports the hypothesis that the compound acts as a competitive AMPA receptor antagonist and is in accordance with the observation that the (2*R*)-form is responsible for both the behavioral and pharmacological activity of IKM-159. Racemic IKM-159 inhibited both neuronal EPSCs and rapid, glutamate-evoked whole-cell currents from recombinant AMPA receptors containing GluA2 and GluA4 with micromolar potency. The mechanism of action was suggested to be competitive antagonism because equilibrium currents were reduced in an agonist-concentration dependent manner, but some uncertainty existed in this interpretation because a physiologically active concentration of IKM-159 (100 μM) failed to displace [$^3$H]AMPA from GluA1, GluA2, or GluA4 AMPA receptors.[9] Here we show that racemic IKM-159 has quite a low binding affinity for full-length GluA2 ($K_i$ of 0.56 mM), consistent with these earlier results. Similar divergences between very low antagonist binding affinity and >10-fold higher potency (for inhibition of receptor activation) have previously been observed for other antagonists derived from the natural product willardiine. For example, UBP282 exhibits a binding affinity at the GluA2 LBD of 0.29 mM (the $IC_{50}$ for displacement of [$^3$H]AMPA)[34] but an $IC_{50}$ of 10 μM for reduction of the fast component of the dorsal-root-evoked ventral root potential (fDR-VRP).[35] UBP282 has a greater number of contacts with the GluA2 binding site residues and is more stable thermally compared to 6-cyano-7-nitroquinoxaline-2,3-dione (CNQX) and 6,7-dinitroquinoxaline-2,3-dione (DNQX), but secondary effects on the entropy of the system as measured by isothermal titration calorimetry likely accounted for the lower binding affinity.[34] It is possible that similar effects underlie the low apparent binding affinity of IKM-159. Finally, we note that the structural and pharmacological data supporting the competitive nature of antagonism by IKM-159 do not exclude the possibility that (2*R*)-IKM-159 has other noncompetitive site(s) of action on AMPA receptors.

Mixed dimers of GluA2 LBD have previously been seen in which glutamate is present in one molecule of the dimer and an antagonist[33,36] or an agonist[37] is found in the other molecule of the dimer. To our knowledge, this is the first time that the structure of a mixed dimer of GluA2 has been solved with an antagonist molecule located in one molecule of the dimer (exhibiting an open domain structure similar to the apo structure and other antagonist structures) whereas the other molecule of the dimer occurs in a partially closed domain structure in which a sulfate ion bridges lobes D1 and D2. As a result, the sulfate-bound molecule assumes a structure slightly more open than that containing the partial agonist kainate.[29] The mixed dimer structure shows the same Ile654−Ile654 linker−linker distance as the GluA2 apo structure (27.6 Å). Thus, binding of only one (2*R*)-IKM-159 molecule within the dimer seems to be enough to capture the dimer in a closed ion channel state. For agonists, the ion channel pore opens when two sites are occupied and the current increases as more binding sites are occupied with agonist.[38] By analogy, the mixed GluA2 dimer with (2*R*)-IKM-159 suggests that in some cases only two subunits need to be occupied by antagonist to block receptor function.

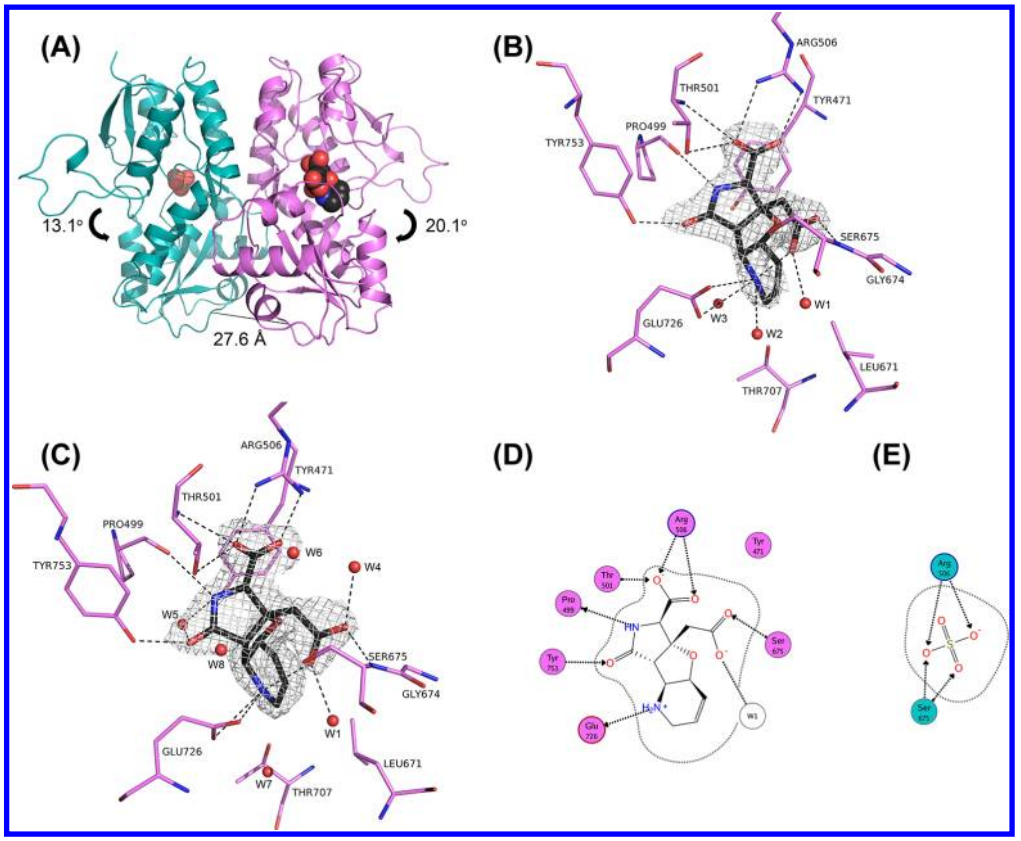


**Figure 5.** Crystal structure of a mixed dimer of GluA2 LBD containing the antagonist (2*R*)-IKM-159 in one molecule of the dimer and a potential sulfate ion in the other molecule of the dimer. (A) Cartoon structure of GluA2 LBD, illustrating the different domain openings induced by (2*R*)-IKM-159 and a sulfate ion, respectively. Also, the Ile654−Ile654 linker−linker distance is indicated. GluA2 LBD with (2*R*)-IKM-159 (molecule A) is shown in violet and with the sulfate ion (molecule C) in cyan. (2*R*)-IKM-159 and the sulfate ion are shown in spheres representation with carbon atoms colored dark gray, nitrogen atoms blue, oxygen atoms red, and sulfur atom yellow. Lobe D1 is located at the top of the figure and lobe D2 at the bottom. (B, C) Zoom on the ligand-binding site of GluA2 LBD with (2*R*)-IKM-159 and $2F_o - F_c$ omit map at 1$\sigma$ carved around the ligand at 1.4 Å radius: (B) molecule A; (C) molecule B. Residues and water molecules within 3.5 Å from (2*R*)-IKM-159 are included. GluA2 is shown in violet and (2*R*)-IKM-159 in dark gray. Heteroatoms are colored as in (A). Potential hydrogen bonds within 3.1 Å from (2*R*)-IKM-159 to water molecules (red spheres) and surrounding residues are shown as black dashed lines. (D) 2D ligand−receptor interaction plot between GluA2 LBD (molecule A) and (2*R*)-IKM-159. The GluA2 residues are shown as violet circles, and contacts from (2*R*)-IKM-159 to the receptor are shown as dotted arrows as calculated by the program MOE [*Molecular Operating Environment (MOE)*, version 2011.10; Chemical Computing Group Inc. (1010 Sherbooke Street West, Suite No. 910, Montreal, Quebec, H3A 2R7, Canada), 2011]. The water molecule in contact with (2*R*)-IKM-159 is shown as a white circle and its contact as a dotted line. (E) 2D ligand−receptor interaction plot between GluA2 LBD (molecule C) and the sulfate ion. The GluA2 residues are shown as cyan circles and contacts between the sulfate ion and the receptor as dotted arrows.

## ■ CONCLUSION

Here we provide a route to the synthesis of (2*R*)-IKM-159, the first characterized member of a novel type of AMPA receptor antagonist. The (2*R*)-IKM-159 was shown to be responsible for the biological activity of the compound, and X-ray structure determination supported that (2*R*)-IKM-159 acts as a competitive antagonist at GluA2. Molecules with this pharmacological activity represent critical tools in neuroscience and continue to be explored as potential therapeutic agents. Generation of new routes of synthesis for IKM-159 and related isomers will facilitate structure−activity relationships that could lead to antagonists with novel activity profiles in future structural and biological studies.

## ■ EXPERIMENTAL SECTION

(2*R*)-IKM-159 (**2**, KT1-121-2) and (2*S*)-IKM-159 (**20**, SG1-146-2) were purified by HPLC using the following conditions: Cosmosyl 20 mm × 250 mm, water 90%, $CH_3CN$ 10% with 0.05% TFA. The peak eluting at 15 min was collected and lyophilized to give pure compound. Final purity of >95% was confirmed by HPLC. For details, see the Supporting Information.

Procedures for all chemical syntheses are described in the Supporting Information.

**Behavioral Assays.** Mice assay was performed under approval by the Ethical Committee of Experimental Animal Care at Hokkaido University, Japan. An aqueous solution (20 $\mu$L) of sample was injected intracerebroventricularly in male ddY mice of 3−4 weeks (22.4 ± 0.96 g, Japan SLC Inc., Hamamatsu) as described previously.[3] Behaviors were observed for up to 8 h, and dose-dependent characteristic behavioral phenotypes were scored as follows: flaccidness (complete loss of righting reflex) lasting for >4 h (score 7), 2−4 h (score 6), 1−2 h (score 5), <1 h (score 4); catalepsy (score 3); loss of voluntary movement as measured by time that a mouse stays still on a stage 6.5 cm diameter and 4.5 cm height (200% of control, score 2; 150−200% of control, score 1; less than 150% of control, score 0). A dose−response curve was generated from the fitted curve from five data points (355, 71, 35, 7, 0.7 nmol/mouse, $n$ = 3 at each dose). Data were analyzed by using the computer software GraphPad Prism.

**Electrophysiology.** Whole-cell patch clamp recordings were carried out from hippocampal neurons isolated from E18 rat pups and cultured for 2−3 weeks under standard conditions, as described previously.[9] To isolate AMPA receptor EPSCs, 50 $\mu$M D-2-amino-5-


dx.doi.org/10.1021/jm301590z | *J. Med. Chem.* 2013, 56, 2283−2293

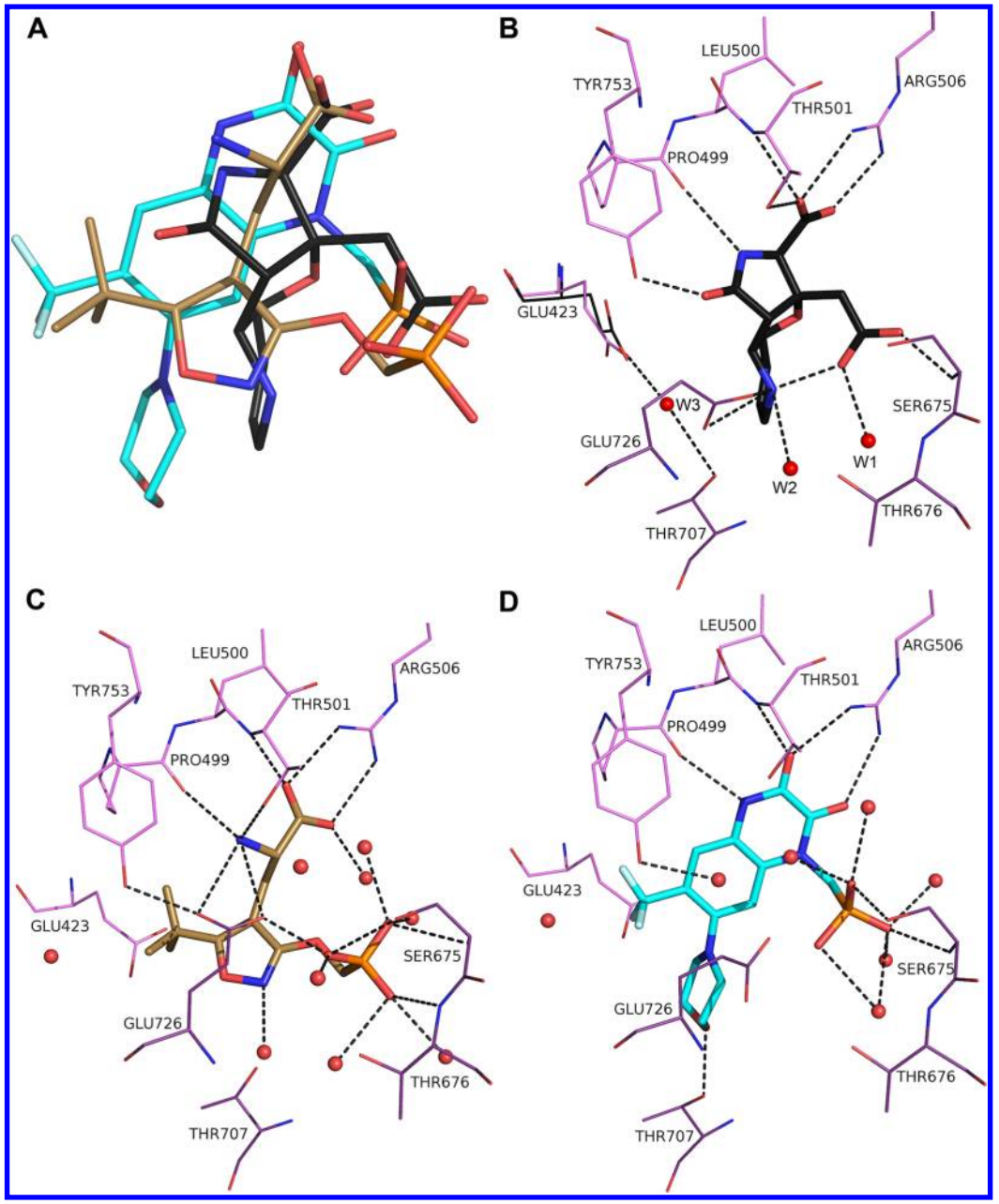


**Figure 6.** Comparison of the structures of GluA2 LBD with (2*R*)-IKM-159, (*S*)-ATPO, and ZK200775, with zoom on the ligand-binding site. The structures have been superimposed on lobe D1 residues. (A) Overlay of (2*R*)-IKM-159 (molecule A, dark gray), (*S*)-ATPO (PDB code 1N0T, molecule A, beige) and ZK200775 (PDB code 3KGC, molecule B, cyan). Nitrogen atoms are blue, oxygen atoms red, and phosphor atoms orange. (B) Structure of GluA2 LBD with (2*R*)-IKM-159 (molecule A). Selected protein residues of lobe D1 are shown in violet and of lobe D2 in dark violet. Glu423 for which the side chain conformation differs in molecules A and B is also shown for molecule B (dark gray). (2*R*)-IKM-159 is shown in dark gray sticks representation, water molecules as red spheres, and potential hydrogen bonds within 3.1 Å as black dashed lines. (C) Structure of GluA2 LBD with (*S*)-ATPO (molecule A). The representation mode is the same as in (B) except that (*S*)-ATPO is shown in beige. The contacts between Glu726 and (*S*)-ATPO are slightly longer than 3.1 Å (3.2−3.3 Å). (D) Structure of GluA2 LBD with ZK200775 (molecule B). The representation mode is the same as in (B) except that ZK200775 is shown in cyan.

phosphonovaleric acid (D-APV), 10 μM bicuculline methiodide, and 50 μM picrotoxin were included in the extracellular bathing solution. CNQX (50 μM) was applied at the conclusion of all recordings to verify that the recorded currents arose from AMPA receptors. Charge transfer during AMPA receptor activations, which in most cases occurred as compound bursts of events, was analyzed in Mini-Analysis, version 6.03 (Synaptosoft) and Clampfit 10 (MDS Software). IKM-159 molecules were bath-applied for 5 min after establishing a stable control recording. Effects of the compounds on AMPA receptor EPSCs were calculated as the charge transfer during the last minute of IKM-159 application relative to that during the last minute of the control period before compound application, expressed as a percentage. A paired Student's *t* test was used to test statistical significance.

**Binding Affinity.** Radioligand binding assays were conducted using (*RS*)-[5-methyl-3*H*]AMPA (45.8 Ci/mmol) (PerkinElmer, MA), as previously detailed.[39] Recombinant baculovirus containing full-length rat GluA2$(R)_o$ was used for infection of Sf9 insect cells, and the membranes were utilized for radioligand binding assays. Non-specific binding at receptors was determined in the presence of 1 mM (*S*)-glutamate. IKM-159 affinity at full-length GluA2$(R)_o$ and GluA2 LBD was determined from competition studies using 1 μM to 2 mM


dx.doi.org/10.1021/jm301590z | *J. Med. Chem.* 2013, 56, 2283−2293

ligand. Competition data were analyzed using Grafit, version 3.00 (Erithacus Software Ltd., Horley, U.K.), as previously detailed.[40]

**Crystallization.** The GluA2 LBD (GluR2-S1S2J)[29] comprises a N-terminal Gly-Ala cloning remnant, amino acid residues 413−527 from segment S1 of the membrane-bound receptor, a Gly-Thr linker, and residues 653−796 from segment S2 (numbering with signal peptide). The protein was expressed and purified as described previously[41,42] except that (*S*)-aspartate was present during purification instead of (*S*)-glutamate. GluA2 LBD in complex with racemic IKM-159 was crystallized using the hanging drop vapor diffusion method at 7 °C. The drop contained 1 μL of protein solution (5.9 mg/mL GluA2 LBD and 6 mM racemic IKM-159 in 10 mM *N*-(2-hydroxyethyl)piperazine-*N*′-ethanesulfonic acid (HEPES), pH 7.0, 20 mM NaCl, and 1 mM ethylenediaminetetraacetic acid (EDTA)) and 1 μL of reservoir solution of 20% PEG4000, 0.1 M lithium sulfate, and 0.1 M phosphate−citrate, pH 4.5. The reservoir volume was 500 μL. The crystals appeared within 1 week, and they were flash cooled with liquid nitrogen after immersion in the reservoir solution containing 20% glycerol.

**X-ray Structure Determination.** Single-crystal X-ray analysis of **8** (2*R*) was performed on a Bruker SMART APEX CCD area (graphite-monochromated Mo K$\alpha$ radiation ($\lambda$ = 0.710 73 Å) with a nitrogen flow temperature controller. Data collection was performed at 183 K. Empirical absorption corrections were applied using the SADABS program [Sheldrick, G. M. *SADABS*; University of Göttingen: Göttingen, Germany, 1996]. The structure was solved by direct methods (SHELXS-97)[43] and refined by full-matrix least-squares calculations on $F^2$ (SHELXL-97)[43] using the SHELX-TL program package. Non-hydrogen atoms were refined anisotropically. Hydrogen atoms were fixed at calculated positions and refined using a riding model. Crystallographic data of the structure are summarized in the Supporting Information. CCDC-900962 contains the supplementary crystallographic data for this paper. The data can be obtained free of charge from The Cambridge Crystallographic Data Centre via http://www.ccdc.cam.ac.uk/data_request/cif.

Data for the crystal structure of GluA2 LBD in complex with (2*R*)-IKM-159 were collected at the I911-3 beamline (MAX-Lab, Lund, Sweden) and processed using XDS[44] and the CCP4 suite of programs.[45] The structure was solved by molecular replacement using PHASER[46] within CCP4 using the structure of GluA2 LBD with (*S*)-ATPO [PDB code 1N0T, molA][32] as a search model. A clear solution comprising four molecules forming two mixed dimers (A/C and B/D, respectively) was obtained. Molecules A and B contain (2*R*)-IKM-159, and molecules C and D contain sulfate or phosphate at the glutamate binding site (has been modeled as sulfate). Afterward, the amino acid residues of GluA2 were automatically modeled into the electron density using ARP/wARP[47] within CCP4 except for a few residues that were manually built using COOT.[48] The output model was further refined in PHENIX.[49] Between every refinement step the structure was checked and modified in COOT. The ligand coordinates were created in Maestro [*Maestro*, version 9.2; Schrödinger, LLC: New York, NY, 2011] and fitted into the electron density. Topology and parameter files for (2*R*)-IKM-159 were obtained using eLBOW[50] after geometry optimization (MMFFs [*MacroModel*, version 9.9; Schrödinger, LLC: New York, NY, 2011]). Water molecules and ions were gradually modeled into the structure. For data collection and refinement statistics, see Table 1. Domain openings were measured relative to the glutamate bound structure of GluA2 LBD (PDB code 1FTJ, molB),[29] using DynDom.[51] Figures were prepared in PyMOL [*The PyMOL Molecular Graphics System*; Schrödinger, LLC: New York, NY, 2006]. The atomic coordinates and structure factors have been deposited at the Protein Data Bank with accession code 4ISU.

## ■ ASSOCIATED CONTENT

### Supporting Information

Synthetic procedure, characterization, and $^1$H and $^{13}$C NMR spectra of new compounds; single-crystal X-ray diffraction experiment of **8** (2*R*); behavioral effects of (2*R*)- and (2*S*)-IKM-159 on mice. This material is available free of charge via the Internet at http://pubs.acs.org.

## ■ AUTHOR INFORMATION

### Corresponding Author

*Phone: +81-45-787-2403. Fax: +81-45-787-2403. E-mail: moikawa@yokohama-cu.ac.jp.

### Notes

The authors declare no competing financial interest.

## ■ ACKNOWLEDGMENTS

The authors thank Prof. S. Nishiyama (Keio University, Japan) for access to the HRMS facility. Heidi Peterson is thanked for help with production of the GluA2 protein. The MAX-Lab, Lund, Sweden, is thanked for providing beam time, and GluTarget and Danscatt are thanked for financial support (to L.J., D.S.P., K.F., and J.S.K.). G.T.S. acknowledges support from the National Institute of Neurological Diseases and Stroke (Grant 2R01NS44322). This work was partly supported by the grant for 2010−2012 Strategic Research Promotion (Nos. T2202, T2309, T2401) of Yokohama City University, Japan. Financial support (a Grant-in-Aid for Scientific Research (Grant 21603004 to M.O, Grants 2238011401 and 231850301 to R.S.)) from the Ministry of Education, Science, Sports, Culture and Technology, Japan, is also gratefully acknowledged.

## ■ ABBREVIATIONS USED

$Ac_2O$, acetic anhydride; AMPA, (*S*)-2-amino-3-(3-hydroxy-5-methyl-4-isoxazolyl)propionic acid; D-APV, D-2-amino-5-phosphonovaleric acid; ATPO, 2-amino-3-[5-*tert*-butyl-3-(phosphonomethoxy)-4-isoxazolyl]propionic acid; Boc, *tert*-butoxycarbonyl; CAN, ceric ammonium nitrate; CNQX, 6-cyano-7-nitroquinoxaline-2,3-dione; CNS, central nervous system; DDQ, 2,3-dichloro-5,6-dicyano-*p*-benzoquinone; DMAP, 4-dimethylaminopyridine; DNQX, 6,7-dinitroquinoxaline-2,3-dione; EDTA, ethylenediaminetetraacetic acid; EPSC, excitatory postsynaptic current; GABA, $\gamma$-aminobutyric acid; HEPES, *N*-(2-hydroxyethyl)piperazine-*N*′-ethanesulfonic acid; iGluR, ionotropic glutamate receptor; KA, kainic acid; LBD, ligand-binding domain; NMDA, *N*-methyl-D-aspartic acid; Ns, 2-nitrobenzenesulfonyl; TMS-$CHN_2$, trimethylsilyldiazomethane

## ■ REFERENCES

(1) Riedel, G.; Platt, B.; Micheau, J. Glutamate receptor function in learning and memory. *Behav. Brain. Res.* **2003**, *140*, 1−47.

(2) Sakai, R.; Koike, T.; Sasaki, M.; Shimamoto, K.; Oiwa, C.; Yano, A.; Suzuki, K.; Tachibana, K.; Kamiya, H. Isolation, structure determination, and synthesis of neodysiherbaine A, a new excitatory amino acid from a marine sponge. *Org. Lett.* **2001**, *3*, 1479−1482.

(3) Sakai, R.; Swanson, G. T.; Shimamoto, K.; Green, T.; Contractor, A.; Ghetti, A.; Tamura-Horikawa, Y.; Oiwa, C.; Kamiya, H. Pharmacological properties of the potent epileptogenic amino acid dysiherbaine, a novel glutamate receptor agonist isolated from the marine sponge *Dysidea herbacea*. *J. Pharmacol. Exp. Ther.* **2001**, *296*, 650−658.

(4) O'Neill, M. J.; Bleakman, D.; Zimmerman, D. M.; Nisenbaum, E. S. AMPA receptor potentiators for the treatment of CNS disorders. *Curr. Drug Targets: CNS Neurol. Disord.* **2004**, *3*, 181−194.

(5) Francis, P. T. The interplay of neurotransmitters in Alzheimer's disease. *CNS Spectrums* **2005**, *10*, 6−9.

(6) Stawski, P.; Janovjak, H.; Trauner, D. Pharmacology of ionotropic glutamate receptors: a structural perspective. *Bioorg. Med. Chem.* **2010**, *18*, 7759−7772.

(7) Ikoma, M.; Oikawa, M.; Gill, M. B.; Swanson, G. T.; Sakai, R.; Shimamoto, K.; Sasaki, M. Regioselective domino metathesis of 7-oxanorbornenes and its application to the synthesis of biologically active glutamate analogues. *Eur. J. Org. Chem.* **2008**, 5215−5220.
(8) Oikawa, M.; Ikoma, M.; Sasaki, M.; Gill, M. B.; Swanson, G. T.; Shimamoto, K.; Sakai, R. Regioselective domino metathesis of unsymmetrical 7-oxanorbornenes with electron-rich vinyl acetate toward biologically active glutamate analogues. *Eur. J. Org. Chem.* **2009**, *2009*, 5531−5548.
(9) Gill, M. B.; Frausto, S.; Ikoma, M.; Sasaki, M.; Oikawa, M.; Sakai, R.; Swanson, G. T. A series of structurally novel heterotricyclic α-amino-3-hydroxyl-5-methyl-4-isoxazole-propionate receptor-selective antagonists. *Br. J. Pharmacol.* **2010**, *160*, 1417−1429.
(10) Oikawa, M.; Ikoma, M.; Sasaki, M.; Gill, M. B.; Swanson, G. T.; Shimamoto, K.; Sakai, R. Improved synthesis and in vitro/in vivo activities of natural product-inspired, artificial glutamate analogs. *Bioorg. Med. Chem.* **2010**, *18*, 3795−3804.
(11) Parsons, A. F. Recent developments in kainoid amino acid chemistry. *Tetrahedron* **1996**, *52*, 4149−4174.
(12) Swanson, G. T.; Sakai, R. Ligands for Ionotropic Glutamate Receptors. In *Marine Toxins as Research Tools*; Fusetani, N., Kem, W., Eds.; Springer: Berlin, 2009; Vol. *46*, pp 123−157.
(13) Oikawa, M.; Kasori, Y.; Katayama, L.; Murakami, E.; Oikawa, Y.; Ishikawa, Y. Biology- and diversity-oriented domino reactions toward ligands for neuronal receptors. Unpublished results.
(14) Nicolaou, K. C.; Boddy, C. N. C.; Li, H.; Koumbis, A. E.; Hughes, R.; Natarajan, S.; Jain, N. F.; Ramanjulu, J. M.; Bräse, S.; Solomon, M. E. Total synthesis of vancomycin—Part 2: Retro-synthetic analysis, synthesis of amino acid building blocks and strategy evaluations. *Chem.—Eur. J.* **1999**, *5*, 2602−2621.
(15) Katritzky, A. R.; Sutharchanadevi, M.; Urogdi, L. Benzotriazol-1-ylalkyl isocyanides: versatile synthons for preparation of unsymmetrical formamidines. *J. Chem. Soc., Perkin Trans. 1* **1990**, 1847−1851.
(16) Mucsi, Z.; Chass, G. A.; Csizmadia, I. G. Amidicity change as a significant driving force and thermodynamic selection rule of transamidation reactions. A synergy between experiment and theory. *J. Phys. Chem. B* **2008**, *112*, 7885−7893.
(17) Takeuchi, R.; Tanabe, K.; Tanaka, S. Stereodivergent synthesis of (*E*)- and (*Z*)-2-alken-4-yn-1-ols from 2-propynoic acid: a practical route via 2-alken-4-ynoates. *J. Org. Chem.* **2000**, *65*, 1558−1561.
(18) Holub, N.; Blechert, S. Ring-rearrangement metathesis. *Chem. Asian J.* **2007**, *2*, 1064−1082.
(19) Fukuyama, T.; Jow, C. K.; Cheung, M. 2-Nitrobenzenesulfonamides and 4-nitrobenzenesulfonamides: exceptionally versatile means for preparation of secondary-amines and protection of amines. *Tetrahedron Lett.* **1995**, *36*, 6373−6374.
(20) Kan, T.; Fukuyama, T. Ns strategies: a highly versatile synthetic method for amines. *Chem. Commun.* **2004**, 353−359.
(21) Cluzeau, J.; Oishi, S.; Ohno, H.; Wang, Z.; Evans, B.; Peiper, S. C.; Fujii, N. Design and synthesis of all diastereomers of cyclic pseudodipeptides as mimics of cyclic CXCR4 pentapeptide antagonists. *Org. Biomol. Chem.* **2007**, *5*, 1915−1923.
(22) Ikoma, M.; Oikawa, M.; Sasaki, M. Synthesis and domino metathesis of functionalized 7-oxanorbornene analogs toward cis-fused heterocycles. *Tetrahedron* **2008**, *64*, 2740−2749.
(23) Garber, S. B.; Kingsbury, J. S.; Gray, B. L.; Hoveyda, A. H. Efficient and recyclable monomeric and dendritic Ru-based metathesis catalysts. *J. Am. Chem. Soc.* **2000**, *122*, 8168−8179.
(24) Bal, B. S.; Childers, W. E., Jr.; Pinnick, H. W. Oxidation of α,β-unsaturated aldehydes. *Tetrahedron* **1981**, *37*, 2091−2096.
(25) Fustero, S.; Mateu, N.; Albert, L.; Aceña, J. L. Straightforward stereoselective access to cyclic peptidomimetics. *J. Org. Chem.* **2009**, *74*, 4429−4432.
(26) Semak, V.; Escolano, C.; Arróniz, C.; Bosch, J.; Amat, M. A practical procedure for the removal of the phenylethanol moiety from phenylglycinol-derived lactams. *Tetrahedron: Asymmetry* **2010**, *21*, 2542−2549.
(27) Ábrahám, G.; Sólyom, S.; Csuzdi, E.; Berzsenyi, P.; Ling, I.; Tarnawa, I.; Hámori, T.; Pallagi, I.; Horváth, K.; Andrási, F.; Kapus, G.; Hársing, L. G., Jr; Király, I.; Patthy, M.; Horváth, G. New noncompetitive AMPA antagonists. *Bioorg. Med. Chem.* **2000**, *8*, 2127−2143.
(28) Turski, L.; Schneider, H. H.; Neuhaus, R.; McDonald, F.; Jones, G. H.; Lofberg, B.; Schweinfurth, H.; Huth, A.; Kruger, M.; Ottow, E. Phosphonate quinoxalinedione AMPA antagonists. *Restor. Neurol. Neurosci.* **2000**, *17*, 45−59.
(29) Armstrong, N.; Gouaux, E. Mechanisms for activation and antagonism of an AMPA-sensitive glutamate receptor: crystal structures of the GluR2 ligand binding core. *Neuron* **2000**, *28*, 165−181.
(30) Pøhlsgaard, J.; Frydenvang, K.; Madsen, U.; Kastrup, J. S. Lessons from more than 80 structures of the GluA2 ligand-binding domain in complex with agonists, antagonists and allosteric modulators. *Neuropharmacology* **2011**, *60*, 135−150.
(31) Laskowski, R. A.; Macarthur, M. W.; Moss, D. S.; Thornton, J. M. PROCHECK—a program to check the stereochemical quality of protein structures. *J. Appl. Crystallogr.* **1993**, *26*, 283−291.
(32) Hogner, A.; Greenwood, J. R.; Liljefors, T.; Lunn, M. L.; Egebjerg, J.; Larsen, I. K.; Gouaux, E.; Kastrup, J. S. Competitive antagonism of AMPA receptors by ligands of different classes: crystal structure of ATPO bound to the GluR2 ligand-binding core, in comparison with DNQX. *J. Med. Chem.* **2003**, *46*, 214−221.
(33) Sobolevsky, A. I.; Rosconi, M. P.; Gouaux, E. X-ray structure, symmetry and mechanism of an AMPA-subtype glutamate receptor. *Nature* **2009**, *462*, 745−756.
(34) Ahmed, A. H.; Thompson, M. D.; Fenwick, M. K.; Romero, B.; Loh, A. P.; Jane, D. E.; Sondermann, H.; Oswald, R. E. Mechanisms of antagonism of the GluR2 AMPA receptor: structure and dynamics of the complex of two willardiine antagonists with the glutamate binding domain. *Biochemistry* **2009**, *48*, 3894−3903.
(35) More, J. C. A.; Troop, H. M.; Dolman, N. P.; Jane, D. E. Structural requirements for novel willardiine derivatives acting as AMPA and kainate receptor antagonists. *Br. J. Pharmacol.* **2003**, *138*, 1093−1100.
(36) Kasper, C.; Pickering, D. S.; Mirza, O.; Olsen, L.; Kristensen, A. S.; Greenwood, J. R.; Liljefors, T.; Schousboe, A.; Watjen, F.; Gajhede, M.; Sigurskjold, B. W.; Kastrup, J. S. The structure of a mixed GluR2 ligand-binding core dimer in complex with (*S*)-glutamate and the antagonist (*S*)-NS1209. *J. Mol. Biol.* **2006**, *357*, 1184−1201.
(37) Vogensen, S. B.; Frydenvang, K.; Greenwood, J. R.; Postorino, G.; Nielsen, B.; Pickering, D. S.; Ebert, B.; Bolcho, U.; Egebjerg, J.; Gajhede, M.; Kastrup, J. S.; Johansen, T. N.; Clausen, R. P.; Krogsgaard-Larsen, P. A tetrazolyl-substituted subtype-selective AMPA receptor agonist. *J. Med. Chem.* **2007**, *50*, 2408−2414.
(38) Rosenmund, C.; Stern-Bach, Y.; Stevens, C. F. The tetrameric structure of a glutamate receptor channel. *Science* **1998**, *280*, 1596−1599.
(39) Nielsen, B. B.; Pickering, D. S.; Greenwood, J. R.; Brehm, L.; Gajhede, M.; Schousboe, A.; Kastrup, J. S. Exploring the GluR2 ligand-binding core in complex with the bicyclical AMPA analogue (*S*)-4-AHCP. *FEBS J.* **2005**, *272*, 1639−1648.
(40) Nielsen, B. S.; Banke, T. G.; Schousboe, A.; Pickering, D. S. Pharmacological properties of homomeric and heteromeric GluR1(o) and GluR3(o) receptors. *Eur. J. Pharmacol.* **1998**, *360*, 227−238.
(41) Ramanoudjame, G.; Du, M.; Mankiewicz, K. A.; Jayaraman, V. Allosteric mechanism in AMPA receptors: a FRET-based investigation of conformational changes. *Proc. Natl. Acad. Sci. U.S.A.* **2006**, *103*, 10473−10478.
(42) Juknaitė, L.; Venskutonytė, R.; Assaf, Z.; Faure, S.; Gefflaut, T.; Aitken, D. J.; Nielsen, B.; Gajhede, M.; Kastrup, J. S.; Bunch, L.; Frydenvang, K.; Pickering, D. S. Pharmacological and structural characterization of conformationally restricted (*S*)-glutamate analogues at ionotropic glutamate receptors. *J. Struct. Biol.* **2012**, *180*, 39−46.
(43) Sheldrick, G. M. A short history of SHELX. *Acta Crystallogr.* **2008**, *A64*, 112−122.

(44) Kabsch, W. XDS. *Acta Crystallogr., Sect. D: Biol. Crystallogr.* **2010**, *66*, 125−132.
(45) Winn, M. D.; Ballard, C. C.; Cowtan, K. D.; Dodson, E. J.; Emsley, P.; Evans, P. R.; Keegan, R. M.; Krissinel, E. B.; Leslie, A. G. W.; McCoy, A.; McNicholas, S. J.; Murshudov, G. N.; Pannu, N. S.; Potterton, E. A.; Powell, H. R.; Read, R. J.; Vagin, A.; Wilson, K. S. Overview of the CCP4 suite and current developments. *Acta Crystallogr., Sect. D: Biol. Crystallogr.* **2011**, *67*, 235−242.
(46) McCoy, A. J.; Grosse-Kunstleve, R. W.; Adams, P. D.; Winn, M. D.; Storoni, L. C.; Read, R. J. Phaser crystallographic software. *J. Appl. Crystallogr.* **2007**, *40*, 658−674.
(47) Cohen, S. X.; Ben Jelloul, M.; Long, F.; Vagin, A.; Knipscheer, P.; Lebbink, J.; Sixma, T. K.; Lamzin, V. S.; Murshudov, G. N.; Perrakis, A. ARP/wARP and molecular replacement: the next generation. *Acta Crystallogr., Sect. D: Biol. Crystallogr.* **2008**, *64*, 49−60.
(48) Emsley, P.; Lohkamp, B.; Scott, W. G.; Cowtan, K. Features and development of Coot. *Acta Crystallogr., Sect. D: Biol. Crystallogr.* **2010**, *66*, 486−501.
(49) Adams, P. D.; Afonine, P. V.; Bunkoczi, G.; Chen, V. B.; Davis, I. W.; Echols, N.; Headd, J. J.; Hung, L. W.; Kapral, G. J.; Grosse-Kunstleve, R. W.; McCoy, A. J.; Moriarty, N. W.; Oeffner, R.; Read, R. J.; Richardson, D. C.; Richardson, J. S.; Terwilliger, T. C.; Zwart, P. H. PHENIX: a comprehensive Python-based system for macromolecular structure solution. *Acta Crystallogr., Sect. D: Biol. Crystallogr.* **2010**, *66*, 213−221.
(50) Moriarty, N. W.; Grosse-Kunstleve, R. W.; Adams, P. D. Electronic ligand builder and optimization workbench (eLBOW): a tool for ligand coordinate and restraint generation. *Acta Crystallogr., Sect. D: Biol. Crystallogr.* **2009**, *65*, 1074−1080.
(51) Hayward, S.; Lee, R. A. Improvements in the analysis of domain motions in proteins from conformational change: DynDom version 1.50. *J. Mol. Graphics Modell.* **2002**, *21*, 181−183.